PCCP

Accepted Manuscript

This article can be cited before page numbers have been issued, to do this please use: M. Boyer, L. Viliauskas and G. S. Hwang, *Phys. Chem. Chem. Phys.*, 2016, DOI: 10.1039/C6CP05140E.

ROYAL SOCIETY OF CHEMISTRY

www.rsc.org/pccp

View Article Online
DOI: 10.1039/C6CP05140E

Structure and Li^+ ion transport in a mixed carbonate/$LiPF_6$ electrolyte near graphite electrode surfaces: a molecular dynamics study

*Mathew J. Boyer, Linas Vilčiauskas, and Gyeong S. Hwang**

McKetta Department of Chemical Engineering, University of Texas, Austin, Texas 78712, USA

Electrolyte and electrode materials used in lithium-ion batteries have been studied separately to a great extent, however the structural and dynamical properties of the electrolyte-electrode interface still remain largely unexplored despite its critical role in governing battery performance. Using molecular dynamics simulations, we examine the structural reorganization of solvent molecules (cyclic ethylene carbonate: linear dimethyl carbonate 1:1 molar ratio doped with 1M $LiPF_6$) in the vicinity of graphite electrodes with varying surface charge densities (σ). The interfacial structure is found to be sensitive to the molecular geometry and polarity of each solvent molecule as well as the surface structure and charge distribution of the negative electrode. We also evaluated the potential difference across the the electrolyte-electrode interface, which exhibits a nearly linear variation with respect to σ up until the onset of Li^+ ion accumulation onto the graphite edges from the electrolyte. In addition, well-tempered metadynamics simulations are employed to predict the free-energy barriers to Li^+ ion transport through the relatively dense interfacial layer, along with analysis of the Li^+ solvation sheath structure. Quantitative analysis of the molecular arrangements at the electrolyte-electrode interface will help better understand and describe electrolyte decomposition, especially in the early stages of solid-electrolyte-interphase (SEI) formation. Moreover, the computational framework presented in this work offers a means to explore the effects of solvent composition, electrode surface modification, and operating temperature on the interfacial structure and properties, which may further assist in efforts to engineer the electrolyte-electrode interface leading to a SEI layer that optimizes battery performance.

*Author to whom correspondence should be addressed: e-mail: gshwang@che.utexas.edu

View Article Online
DOI: 10.1039/C6CP05140E

I. Introduction

With the global movement towards a CO_2-free economy and the rapid growth in intermittent renewable energy, energy storage is more important now, than ever. Since their inception, lithium-ion batteries (LIB) have aided the technological revolution of portable electronic devices. A similar long sought-after revolution is anticipated in the automotive industry. Unfortunately, the current LIBs severely limit battery-powered electric vehicles to short-range commuting because of their low energy densities and charge rates. Despite a broad spectrum of work to develop new storage concepts and transition to more sustainable materials, LIBs remain the state-of-the-art in the area of electrochemical energy storage. Gaps between theoretical and actual performance in current LIBs highlight the need for further understanding to improve existing technologies as well as to develop new energy storage concepts.[1–6]

Modern LIBs are typically comprised of transition metal oxide cathodes, graphitic carbon anodes, and electrolytes containing inorganic lithium salts dissolved in small molecule organic solvents. However, typical organic solvents (carbonates, ethers, etc.) and salt anions (PF_6^-, BF_4^-, ClO_4^-, etc.) are not electrochemically stable at the graphite electrode surface and may undergo decomposition to form a passivating layer, typically labeled as the solid-electrolyte interphase (SEI).[7–10] The electrode and electrolyte materials have been studied separately to great extents, but it is at the interfaces where the key electrochemical processes occur which govern battery performance.[2,8,10–28] Therefore, a fundamental (molecular level) understanding of thermodynamics, transport phenomena, and electrochemical reactions at the electrolyte-electrode interface is crucial for the further advancement of battery technologies.

Due to the transient nature of electrochemical processes in LIBs, real-time *in situ*[29] characterization is preferable, especially since an *ex situ postmortem* study may fail to capture

View Article Online
DOI: 10.1039/C6CP05140E

real-time dynamics.[5] Moreover, owing to the size and time scales of the electrolyte-electrode interfacial phenomena, there are only a few experimental techniques able to provide the appropriate resolution. Alternatively, computational studies may allow the system to be observed at (across) spatial (temporal) scales often unavailable in experiments.[30–38]

Molecular modeling techniques have been extensively used to understand the fundamentals of electrochemical and transport processes in LIB systems. First principles methods, usually based on the density functional theory (DFT), are able to provide unprecedented fundamental details on the interfacial structure and dynamics, such as lithium diffusion and intercalation, solvent reorganization and decomposition, and so forth. Although the first-principles approach can effectively describe complex electrochemical processes,[30–35] the high computational cost restricts its application to systems of no more than several hundred atoms with trajectories of tens of picoseconds. Classical force field calculations, on the other hand, lack the chemical nature, but well reproduce many structural and dynamical properties of materials while simulating tens of thousands of atoms over hundreds of nanoseconds. Force field-based molecular dynamics (MD) studies have already been used to explore the nature of bulk electrolytes[36] as well as lithium ion behavior at various interfaces.[37,38] Vatamanu *et al*.[37] examined the effect of electrode potential on the structure of a mixed carbonate/$LiPF_6$ electrolyte near the basal surface of graphite. While graphite edge-planes have been shown to have several orders of magnitude higher electron transfer rates[39] and are thus expected to dominate the salient reaction chemistries found in LIBs, Jorn *et al*.[38] considered both basal and flat edge-planes but only for a single carbonate electrolyte, and Jow *et al*.[40] reported free energy profiles calculated as a function of Li^+ position in a mixed carbonate/$LiPF_6$ electrolyte near a uncharged graphite edge-plane.

View Article Online
DOI: 10.1039/C6CP05140E

In this work, we employ classical MD simulations to investigate the structural reorganization of EC:DMC(1:1)/$LiPF_6$ 1M due to the interaction with edge-plane graphite surfaces, along with the resulting potential difference across the electrolyte-electrode interface as well as Li^+ ion transport through the interfacial layer. We first predict the near-interface EC/DMC/Li^+/PF_6^- distributions with varying charge densities on the hydrogen-terminated graphite edges. From the resulting structures, we also estimate the variation of the potential difference across the electrolyte-electrode interface as well as the relation between applied voltage and electrode surface charge density. Then, we evaluate the transport rate of Li^+ by calculating the free-energy penalties associated with its moving to the interface from the bulk region using advanced sampling techniques (metadynamics) to understand how the interfacial structure affects Li^+ ion dynamics. This theoretical study aims at gaining a deeper understanding of the nature of molecular interactions at the interfaces between carbonate-based mixed solvent electrolytes and graphite electrodes, especially the reorganization of solvent molecules due to electrode charging.

Nowadays it is common practice to utilize binary and even ternary mixtures of carbonate solvents to balance lithium salt solubility and viscosity; this provides an additional degree of freedom which has been largely neglected in the study of SEI formation and Li^+ ion transport. Our study clearly demonstrates that the composition and structural ordering of the mixed electrolyte in proximity to the interface are substantially different from those in the bulk. Quantitative prediction of the interfacial structure is essential to better understanding electrolyte decomposition/diffusion processes along with Li^+ ion dynamics near the electrode, especially at the onset of SEI formation that may signficantly influence its growth which is known to be kinetically governed. The improved understanding may further assist in efforts to engineer the

View Article Online
DOI: 10.1039/C6CP05140E

electrolyte-electrode interface leading to an SEI which optimizes LIB performance.

II. Computational methods

A. Classical molecular dynamics

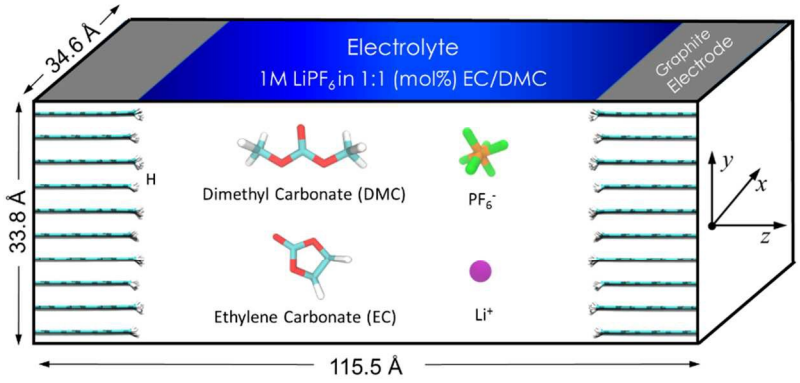

Figure 6. Schematic of the simulation cell. The electrolyte solution contains 1M $LiPF_6$ in EC:DMC (= 1:1 molar ratio) and the negative electrode is modelled as a stack of ten graphene nanoribbons with hydrogen-terminated zigzag edges. For EC, DMC, and PF_6^-, white, red, blue, orange, and green colors represent H, O, C, P, and F, respectively. Periodic boundary conditions are applied in the *x*, *y* and *z* directions.

We performed MD simulations with the OPLS-AA force field[41–43] using the GROMACS simulation package (version 4.6.7)[44]. As illustrated in Figure 6, simulations with periodic boundary conditions were conducted using a system representing the half-cell of the anode side in a LIB; the rectangular simulation cell is comprised of a liquid electrolyte (1M $LiPF_6$ in EC:DMC (= 1:1 molar ratio)) and a negative electrode (which is modelled as a stack of ten graphene nanoribbons with hydrogen-terminated zigzag edges). The nanoribbon sheets are staggered in an ABAB pattern due to the van der Waals interaction between them, yielding a regular corrugated face. The graphite electrode has 3920 carbon atoms in 35 Å × 34 Å × 32 Å; several C atoms in each sheet were restrained with a harmonic potential to prevent significant slip. The electrolyte side consists of 375 DMC and 375 EC molecules in addition to 57 PF_6^-

View Article Online
DOI: 10.1039/C6CP05140E

anions; the number of Li^+ cations is varied depending on the amount of excess charge added to the negative electrode; the excess negative charge was assumed to be uniformly distribute throughout the edge C atoms.

A MD timestep of 1 fs was used in all simulations. The short-range interactions were computed with a spherical cutoff of 1.2 nm, while the long-range electrostatics were accounted for using the particle mesh Ewald (PME) summation method. The systems were initially equilibrated in the NPT ensemble[45,46] and then subsequently annealed in the NVT ensemble[47] at 700 K for 1 ns. After the quench for 0.5 ns, the production runs using various algorithms were carried out at 300 K and comprised a total of more than several hundreds of nanoseconds.

B. Metadynamics

We used well-tempered metadynamics[48,49] to reconstruct the free energy profile associated with Li^+ ion transport through the interfacial layer. The enhanced sampling is performed by biasing a low-dimensional collective variable (CV) which, in our case, is the position *z* from the electrolyte-electrode interface. The metadynamics was performed using the GROMACS simulation package[44] and the PLUMED plugin[50]. The bias is represented by a history-dependent potential constructed as a sum of Gaussian distributions centered along the trajectory in the CV pace:

$$V(\vec{s},t) = \sum_{t'=0,\tau,2\tau,\ldots}^{t'<t} We^{\frac{-V\left(s(q(t'),t')\right)}{\Delta T}} \exp\left(-\sum_{i=1}^{d} \frac{\left(s_i(q)-s_i(q(t'))\right)^2}{2\sigma_i^2}\right) \quad (1)$$

The bias potential pushes the system out of local minima and forces it to explore new regions of the phase space. Furthermore, in the long time limit, the bias potential converges to free energy $-A(\mathbf{s})$ as a function of the CVs:

$$V(\mathbf{s}, t \to \infty) = -A(\mathbf{s}) + C \quad (2)$$

View Article Online
DOI: 10.1039/C6CP05140E

The metadynamics algorithm is essentially controlled by only four parameters: Gaussian deposition stride τ, width σ_i, height $W(k\tau)$ of the Gaussian, and ΔT which controls the rate of Gaussian height decay over the simulation by the well-tempered algorithm.[49]

III. Results and discussion

A. Electrolyte distribution near uncharged electrodes

Figure 1(a) shows the number density (ρ_n) profiles with a bin size of 0.15Å for electrolyte components (based on each molecule's center of mass) along the direction normal to the electrode surface. DMC and EC are found to pack more densely at the interface by approximately 3 and 2 times higher than their bulk values, respectively, which is apparently attributed to the van der Waals (vdW) force at the electrolyte-electrode interface. The preference towards DMC arises from the relatively stronger vdW interactions due to the bulky methyl groups in DMC. The oscillations in ρ_n appear to dampen after about 2 nm to the bulk-like densities.

The first Li^+ peak occurs near 0.7 nm where the ρ_n of both EC and DMC shows a minimum value, while the intensity is noticeably lower than the bulk-like density. This implies that it is relatively difficult for the densely packed carbonate complexes near the electrode to rearrange and solvate Li^+ ions; note that the first solvation shell of Li^+ in the bulk phase contains four carbonate molecules and a PF_6^- anion, as illustrated in the inset of Figure 1(a). The small but distinct second maximum of the first peak at z = 0.55 nm for both EC and DMC is due to the ordering of these molecules around the Li^+ concentrated near 0.7 nm. The second peak at z = 0.82 nm is a result of the interplay between the vdW interactions with the first-layer carbonates and the solvation of Li^+. Due to their electrostatic attraction, PF_6^- organize around the Li^+

View Article Online
DOI: 10.1039/C6CP05140E

leading to the alternative anion/cation layering, as also commonly seen in ionic liquids[51], despite the vastly different electrolyte.

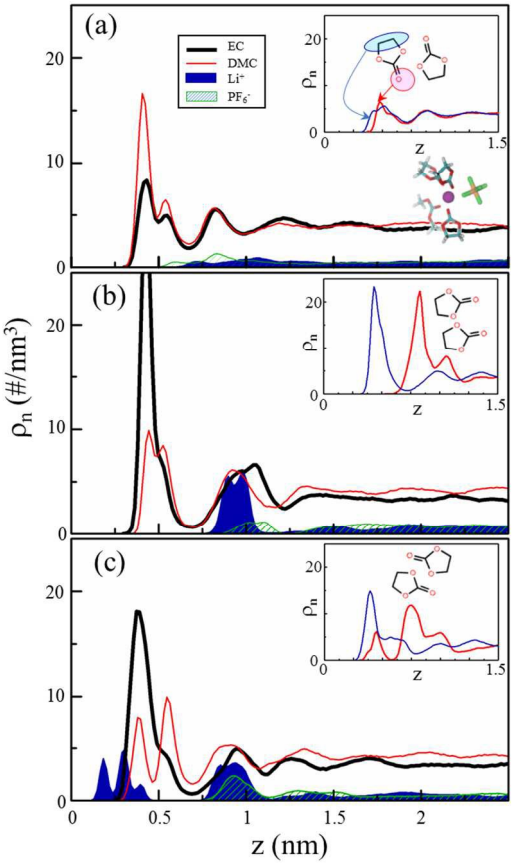

Figure 1. EC, DMC, Li^+ and PF_6^- number density (ρ_n) profiles along the *z*-direction near graphite electrodes with surface charge densities of (a) σ = 0 $\mu C/cm^2$, (b) σ = -11.6 $\mu C/cm^2$, and (c) σ = -16.4 $\mu C/cm^2$. In each inset, the ρ_n profiles for the carbonyl oxygen (red line) and ethylene group (blue line) of EC are also presented to demonstrate changes in the molecular orientation, as illustrated by the 2D EC representations. As shown in (a), the first solvation shell of Li^+ in the bulk-like region commonly consists of four carbonate molecules and one PF_6^- anion.

B. Electrolyte distribution near charged electrodes

To imitate the charge injection in the graphite anode by an applied external voltage, we assigned excess negative charge equally to the electrolyte-adjacent carbon atoms in the electrode; the charge density (σ) was varied between 0 and -16.4 $\mu C/cm^2$. Such representation should be

View Article Online
DOI: 10.1039/C6CP05140E

adequate for mimicking the preferential accumulation of excess charges at the metallic graphite edges, as well demonstrated by previous DFT studies[52]. In order to maintain charge neutrality in the model systems considered, additional Li^+ ions were added to the bulk electrolyte to compensate for the excess negative charge in the electrode.

A charged electrode creates an electric field, which causes the rearrangement of electrolyte components near the electrode to screen the electric field. Figure 1 shows the arrangement of the electrolyte components at σ = 0 $\mu C/cm^2$ [(a)], -11.6 $\mu C/cm^2$ [(b)], and -16.4 $\mu C/cm^2$ [(c)]; additional ρ_n profiles at σ = -4.1 $\mu C/cm^2$ and -8.2 $\mu C/cm^2$ are also presented in the Supporting Information (see Figure S3). At σ = -11.6 $\mu C/cm^2$ [(b)], the first peaks of both EC and DMC shift towards the electrode, indicating a higher degree of alignment. The first-peak intensity of EC (DMC) at z = 0.43 nm increases (decreases) by four (two) times, in comparison to the charge neutral case. As illustrated in the inset of Figure 1(b), the positively charged ethylene group of EC is aligned towards the negatively charged electrode and its carbonyl group towards the bulk. The relatively smaller vdW volume of EC allows it to pack more densely than DMC in the vicinity of the electrode, thereby more effectively screening the electric field from the charged anode; note also that DMC has its positive charge spread over two terminal methyl groups. The alignment of the carbonyls in EC away from the electrode results in an accumulation of Li^+ at z = 0.9 - 1 nm of about 10 times the bulk, which in turn attracts PF_6^- anions leading to the alternative Li^+/ PF_6^- layering.

When σ = -16.4 $\mu C/cm^2$ [(c)], Li^+ begin to accumulate at the graphite edges as the EC/DMC solvent molecules are unable to pack densely enough to shield the charged electrode. The ρ_n profile of Li^+ exhibits two distinct peaks at z = 0.19-0.4 nm and 0.85-0.95 nm. The first peak shows three maxima largely due to the corrugation and hydrogen terminations at the graphite

View Article Online
DOI: 10.1039/C6CP05140E

edges (rendering multiple stable sites for Li^+ depending on its coordination). In this case, Li^+ cations at the interface tend to be partially solvated by EC (and DMC) carbonyl O (z = 0.45 nm), while the majority of EC molecules still remain perpendicular to the electrode edge with their carbonyl group around z = 0.75 nm. The orientation of EC molecules has been shown to be related to the favorability of their decomposition.[53] As Li^+ accumulates on the electrode, the ρ_n of EC (DMC) decreases (increases) in the first layer.

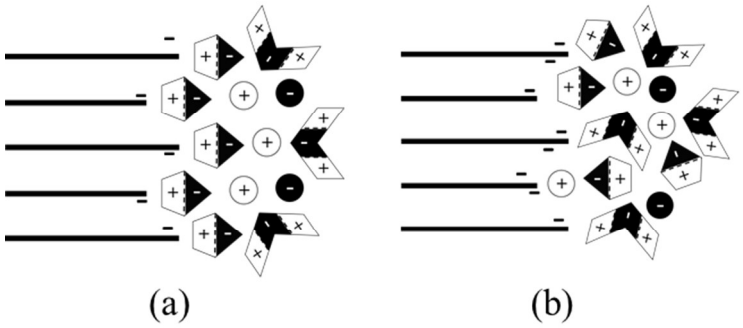

Figure 2. Schematic illustrations of the reorganization of solvent molecules near graphite anodes with (a) moderately and (b) highly charged surfaces. Cyclic ethylene carbonate (EC) and acyclic dimethyl carbonate (DMC) are depicted by a pentagon and a chevron, respectively, while their polarization is indicated by the minus and plus signs. Filled and open circles respectively represent PF_6^- anions and Li^+ cations.

A schematic shown in Figure 2 illustrates the effect of Li^+ accumulation on the electrolyte packing near the interface. In the case of σ = -11.6 $\mu C/cm^2$ [(a)], the first layer mainly consists of EC with carbonyls oriented towards the bulk, leading to the distinct alternating layers of charged groups/ions normal to the electrode. When σ = -16.4 $\mu C/cm^2$ [(b)], the presence of Li^+ at the graphite edges causes a local rearrangement of EC to partially solvate Li^+, and thus the layering behavior is suppressed due to the charge variations occurring not only perpendicular, but also parallel to the electrode.

View Article Online
DOI: 10.1039/C6CP05140E

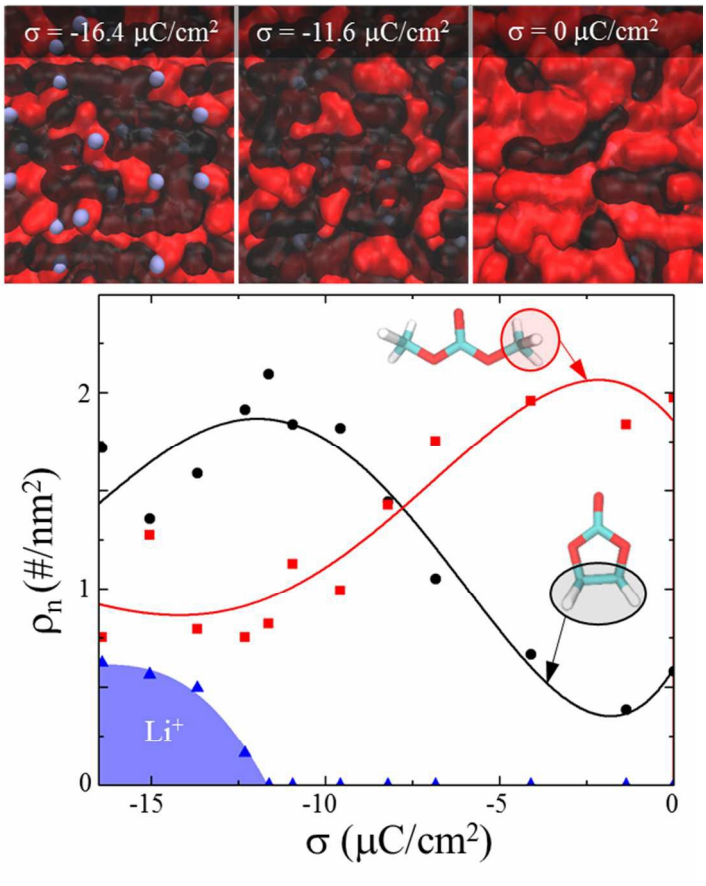

Figure 3. Variations in the number density (ρ_n) of Li^+ and positively charged ethylene/methyl groups (in EC/DMC, as shown by the models) in contact with the electrode at varying surface charge densities (σ). In upper panels, MD snapshots are also shown to visualize the rearrangement of electrolyte species near the negatively charged electrode surfaces. Red/black isosurfaces represent DMC/EC-enriched regions and small blue balls indicate Li^+ cations. DMC which is predominant at σ = 0 μC/cm^2 is gradually replaced by EC with increasing $|\sigma|$, and eventually Li^+ begins to accumulate on the electrode surface.

This analysis shows that the electric field created by the electrode's excess charge is shielded by the positively charged ethylene (and methyl) groups of EC (and DMC) and Li^+ cations, depending on its magnitude. To demonstrate their relative contributions, the integrated ρ_n of the EC ethylene group, DMC methyl group, and Li^+ in the vicinity of the electrode are plotted as a function of σ (see Figure 3). At neutral or slightly charged electrodes, DMC methyl groups exceed EC ethylene groups, but as the amount of the excess charge increases the latter

View Article Online
DOI: 10.1039/C6CP05140E

become more populated than the former. A similar trend was shown by Vatamanu *et al*. [37] near graphite basal surfaces where the EC concentration was shown to monotonically increase with increasingly negative potentials. However, beyond the maximum packing density of EC at the edge-plane, Li^+ begins to accumulate while the ρ_n of EC ethylene (DMC methyl) groups decreases (increases). This finding may serve as a useful benchmark for comparison of structural evolution of electrolytes at the electrode vicinity during the charging process. Understanding the molecular structure of the electrolyte-electrode interface for different electrolyte compositions under various operating conditions can also lend towards a greater understanding of the formation and growth of SEI, particularly during early stages.

C. Variation in potential difference across the electrolyte-electrode interface

From the interfacial structures described in the previous section, we estimated the variation of the potential drop (ϕ) from the metallic electrode to the bulk electrolyte with varying σ until the onset of Li^+ ion accumulation on the electrode surface. We obtained ϕ by solving Poisson's equation in one dimension ($\nabla^2\phi = -\rho/\varepsilon_0$) with boundary conditions of $\phi = 0$ V and $\nabla\phi = 0$ in the bulk region of the electrolyte, where ε_0 is the vacuum permittivity and ρ is the charge density (which is given by weighting the ρ_n for each atom by its charge value and summing them together). For a reference point, we considered the potential of zero charge (PZC, ϕ_Z) which is known to be approximately 3 V *vs*. Li^+/Li(s) (or 0 V *vs*. standard hydrogen potential)[54,55]. The PZC is due to a charge imbalance arising from the vdW interactions between the graphite edges and electrolyte molecules. From our classical MD simulations, the predicted ϕ_Z is about -0.10 V as a result of the excess of positive methyl and ethylene groups at the interface. A similar ϕ_Z value ($\approx$ -0.14 V) was predicted for a flat graphite edge-plane against 1M $LiPF_6$ in pure EC.[38]

View Article Online
DOI: 10.1039/C6CP05140E

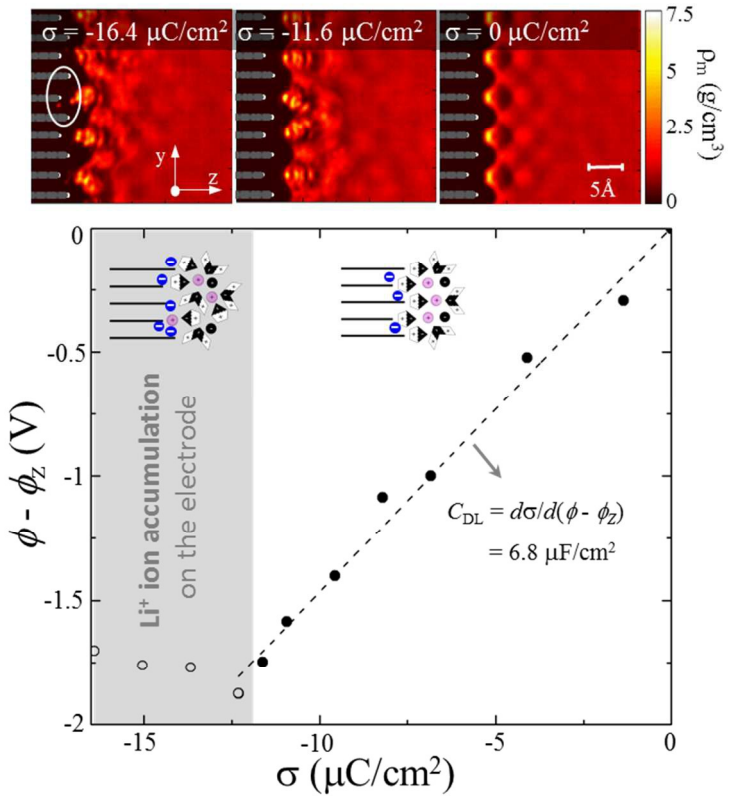

Figure 4. Variations in the potential drop ($\phi - \phi_z$) across the electrolyte-electrode interface as a function of electrode surface charge density (σ). In upper panels, mass density (ρ_m) maps are also shown to visualize perturbations in the spatial distributions of the electrolyte components due to irregular electrode surfaces with rough edges and Li^+ ions accumulated at the graphite edges; the perturbation becomes stronger as the electrode surface is more negatively charged. The inset illustrations show the accumulation of Li^+ ions at the corrugated edges when $\sigma > -12$ $\mu C/cm^2$, which leads to compensation of excess negative charges on the electrode.

As shown in Figure 4, the predicted potential difference ($|\phi - \phi_Z|$) monotonically increases with σ up until $\sigma \approx -12$ $\mu C/cm^2$ (where Li^+ ions begin to precipitate on the electrode surface). Although the data are somewhat scattered, the ($\phi - \phi_Z$) *vs.* σ plot appears to be nearly linear. From the linear plot, the differential capacitance of the electrical double layer formed at the interface is approximated to be $C_{DL} = 6.8$ $\mu F/cm^2$ [$= d\sigma/d(|\phi - \phi_Z|)$], in comparison to the 4-5 $\mu F/cm^2$ reported for a similar electrolyte at a graphite basal surface[37]. Beyond $\sigma = -12$ $\mu C/cm^2$, there is no significant variation in $\phi - \phi_Z$ since the additional excess of negative charge on the

View Article Online
DOI: 10.1039/C6CP05140E

electrode can be compensated by the positive charge of adsorbed Li^+ ions at the corrugated edges, as illustrated in the inset.

Now we should point out that this analysis is based on the assumption that no redox reactions would occur at the electrolyter-electrode interface, like non-Faradaic supercapacitors. However, electrolytes containing EC and Li^+/PF_6^- salts have been reported to undergo decomposition around 0.8 V *vs*. Li^+/Li(s), depending on electrolyte composition[56]; very recently, it was also reported that the reduction of EC:DMC/$LiPF_6$ could occur as high as 1.7 V *vs*. Li^+/Li(s), which was suggested to be related to anion decomposition[57]. For the system considered here, we could approximate the applied voltage (with respect to the potential of the bulk electrolyte) in terms of $(\phi - \phi_Z)$ and the electrode potential (ϕ_E), i.e., $\phi_a = (\phi - \phi_Z) + \phi_E$.[51,52,58,59] From our previous work[52], ϕ_E is approximated to be -0.45 (0.55) V when $\sigma \approx$ -12 (16) $\mu C/cm^2$ at the H-terminated graphene edges. Taking ϕ_E = -0.45 V and $(\phi - \phi_Z)$ = -1.75 V (from Figure 4), the applied voltage is roughly -2.2 V (or 0.8 V *vs*. Li^+/Li(s)) when $\sigma \approx$ -12 $\mu C/cm^2$. This implies that ϕ_a may begin to fall within 0.7-0.9 V *vs*. Li^+/Li(s) (as previously measured for the EC reduction potential on graphite electrodes) when σ reaches above -10 $\mu C/cm^2$. Although there is room for improvement in prediction of the potential values, especially considering charge polarization at the interface[59], at least we can expect that there would be no significant decomposition of solvent molecules while the graphite electrode is charged up until $\sigma \approx$ -10 $\mu C/cm^2$. Beyond this, perhaps solvent molecules at the interface might undergo decomposition during the first charge cycle. However, this process may not occur instantaneously across the entire electrode surface as it becomes negatively charged, depending on the arrangements of solvent molecules. This implies a value to quantifying the structure of the electrolyte at the interface over a range of applied voltages where the reduction reactions would occur.

View Article Online
DOI: 10.1039/C6CP05140E

Additionally, our study shows that the relation between ϕ_a and σ as well as critical σ (or $\phi - \phi_Z$) for interfacial Li^+ precipitation can be strongly influenced by electrolyte composition and temperature (which directly affect solvation of Li^+ ions), along with electrode surface properties. This analysis also highlights the importance of the interfacial structure in characterizing ion mobility, which may be crucial to understanding SEI formation and charge rate.

D. Effect of interfacial structure on Li^+ ion transport

As discussed in the previous section, a Li^+ cation is solvated by a combination of EC, DMC, and PF_6^-. The composition and structure of the Li^+ solvation sheath may vary depending on the solvent composition as well as the relative strength of intermolecular interactions between Li^+-solvent and solvent-solvent. In the bulk electrolyte, the solvated Li^+ may undergo thermally activated random-walk migration, which can be quantified by computing the mean-square displacement or the velocity autocorrelation function of the moving Li^+. The mean-field approach is adequate in describing diffusion when the system is relatively uniform. As demonstrated earlier, however, the electrolyte composition is not spatially uniform and its structure becomes even solid-like near the electrode surface. Hence, other techniques may be required in order to characterize Li^+ solvation and transport properties in the electrolyte-electrode interface region.

The transport rate of Li^+ through the interfacial layer is related to the free-energy penalties associated with its moving from the bulk region. We calculated the relative free energy (ΔA) profiles for a Li^+ ion travelling from the bulk electrolyte to the electrode surface using well-tempered metadynamics simulations. As presented in Figure 5, three different charge states of the electrode were considered to examine the effect of the interfacial structure on Li^+ transport; σ

View Article Online
DOI: 10.1039/C6CP05140E

= 0 μC/cm^2 [(a)], -11.6 μC/cm^2 [(b)], and -16.4 μC/cm^2 [(c)]. For each system, the result was obtained from a 70 ns simulation conducted with an initial Gaussian height of 10 kJ/mol, Gaussian σ of 0.05 nm, ΔT = 7200K, and with Gaussians deposited every 100 fs.

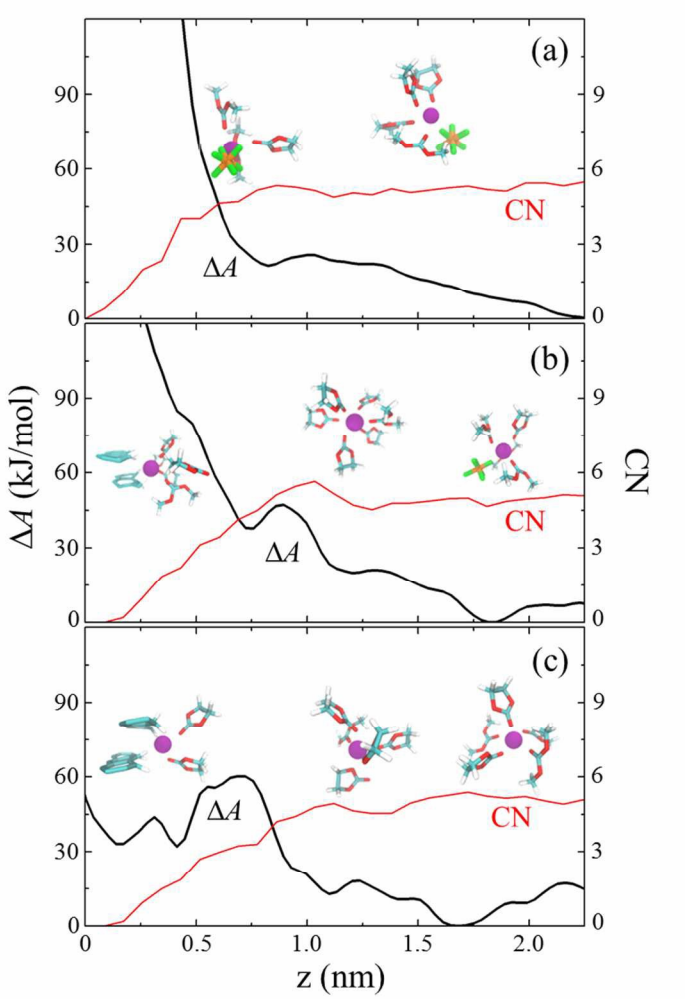

Figure 5. Variations in the relative free energy (ΔA) (left axis) and the Li^+ coordination number (CN) (right axis) along the z-direction near graphite electrodes with surface charge densities of (a) σ = 0 μC/cm^2, (b) σ = -11.6 μC/cm^2, and (c) σ = -16.4 μC/cm^2. Selected screenshots of the Li^+ solvation sheath are also shown to visualize changes in the interaction between Li^+ and neighboring solvent molecules as it moves towards the interface from the bulk-like region.

1. Near Uncharged Electrodes.

When σ = 0 μC/cm^2 [(a)], as Li^+ moves towards the interface from the bulk-like region, the ΔA gradually increases to a maximum around z = 1 nm followed by a slight minimum around z =

View Article Online
DOI: 10.1039/C6CP05140E

0.8 nm, and then there is a rapid increase in ΔA. The energy penalties can be associated with rearrangement of solvent molecules and partial desolvation of Li^+. In the region from z = 2.25 nm to 1 nm, the predicted Li^+ coordination number (CN) is nearly unchanged, suggesting that the Li^+ may remain fully solvated while diffusing through the electrolyte layer. This also implies that at least part of the primary solvation sheath would move with the Li^+, rather than a passing of the Li^+ over the EC/DMC carbonyls via a ratchet mechanism (which would be well represented by oscillations in the CN as the Li^+ passes through transition states). We attribute the gradual increase of ΔA to the increasing energy cost for rearrangements of the Li^+ solvation sheath and its surrounding molecules as the electrolyte becomes more ordered with decreasing z; recall that the layered structure induced by the electrolyte-electrode interaction extends up to $z \approx$ 2.5 nm, as shown in Figure 1.

It is also interesting to note that the maximum (minimum) of ΔA at $z \approx 1$ nm (0.8 nm) corresponds to a minimum (maximum) in ρ_n for EC/DMC (see Figure 1). In addition, the relatively high concentration of PF_6^- anions at z ≈ 0.8 nm may contribute to lowering ΔA by interacting with the Li^+ cation. Below z = 0.8 nm, the sharp increase in ΔA is largely attributed to the Li^+ desolvation as evidenced by the decrease in CN (Figure 5). In the densely packed solid-like layer, the Li^+ may travel as a partially-solvated ion as solvent molecules are unable to rearrange to fully solvate it, bearing a high energy penalty. Here, we could not exclude the possibility that the non-polarizable force fields employed may lead to overestimation of ΔA. Nonetheless, our analysis at least suggests that, in the absence of favorable electrostatic interactions with the electrode, the Li^+ is highly unlikely to diffuse through the densely packed interfacial layer.

View Article Online
DOI: 10.1039/C6CP05140E

2. Near Charged Electrodes.

For both σ = -11.6 $\mu C/cm^2$ [(b)] and -16.4 $\mu C/cm^2$ $\mu C/cm^2$ [(c)] cases, the CN of Li^+ changes minimally as Li^+ moves up to $z \approx 1$ nm from the bulk-like region, implying that the Li^+ can undergo migration while remaining fully solvated. However, unlike the uncharged case [(a)], the ΔA profile exhibits fluctuations along the z direction rather than monotonic increases; the fluctuations appear to become stronger in case (c) compared to case (b). We attribute the ΔA fluctuations largely to perturbations in the spatial distributions of the electrolyte constituents, as demonstrated in the 2D density maps (Upper panels in Figure. 4).

In case (b), the pronounced maximum of ΔA around z = 0.9 nm appears related to the increased ρ_n of EC/DMC/PF_6^- between z = 0.8 nm and 1.1 nm, which may in turn allow Li^+ ions to accumulate in the region while solvating them more tightly as indicated by the increased ρ_n and CN of Li^+. Therefore, we can expect that Li^+ ionic transport through the tightly packed region will be significantly impeded. Due to a similar reason, the ΔA profile tends to exhibit a shoulder around z = 1 nm in case (c).

Below z = 0.8 nm, for both cases (b) and (c), the CN of Li^+ is found to monotonically decrease with decreasing z. This indicates that in the densely packed solid-like layer the Li^+ may travel as a partially-solvated ion as solvent molecules are unable to rearrange to fully solvate it, bearing a high energy penalty. In contrast to case (a), the rather disordered interface layer may help stabilize the Li^+ to a certain degree while it becomes more solid-like with increasing the electrode's charge density (σ); the perturbation effect is likely to be stronger in case (c), relative to case (b), due to the irregularly distributed Li^+ ions at the electrode surface as evidenced by the comparison between corresponding density maps. In case (c), such perturbations in the first electrolyte layer also likely allow for favorable electrostatic interactions with the negatively

View Article Online
DOI: 10.1039/C6CP05140E

charged electrode, thereby stabilizing the partially desolvated Li^+ and thus substantially reduce the energy cost ΔA from 85 kJ/mol to 60 kJ/mol. It would be interesting to note that the predicted Li^+ transport barriers are comparable with 50-80 kJ/mol (depending on electrolyte composition) as reported by previous experimental and theoretical studies[13–15,40] , despite different interfacial and operating conditions.

IV. Conclusions

Molecular dynamics (MD) simulations were used to investigate changes in the distribution of a mixed solvent electrolyte (1M $LiPF_6$ in ethylene carbonate (EC):dimethyl carbonate (DMC) (= 1:1 molar ratio)) in the vicinity of graphite electrodes with varying surface charge densities (σ). From the interfacial structures, we estimated the variation of the potential difference across the electrolyte-electrode interface with respect to σ, along with the relation between applied voltage and σ. In addition, we evaluated Li^+ ion solvation and transport in the ordered and densely-packed interfacial layer by carefully analyzing the solvation sheath structure of Li^+ (such as its coordination number, CN) as well as the free-energy penalties (ΔA) associated with its moving to the interface from the bulk-like region using advanced sampling techniques (well-tempered metadynamics). The goals of this work were to gain a deeper understanding of the interfacial interactions at the molecular level between mixed carbonate-based electrolytes and graphite electrodes, and to provide some intuition to help better understand the fundamental processes involved in SEI formation along with Li^+ ion dynamics at the electrolyte-electrode interface.

Our main findings are summarized below.

View Article Online
DOI: 10.1039/C6CP05140E

- DMC and EC pack densely near the uncharged electrode by approximately 3 and 2 times higher than their bulk values due to the van der Waals (vdW) interaction with the electrode. The preference towards DMC is largely attributed to its bulky methyl groups. After about z = 2 nm from the electrolyte-electrode interface, the electrolyte tends to become bulk-like.
- When the electrode is negatively charged, cyclic EC is found to become more populated than linear DMC. We attribute this to the relatively smaller size of EC that allows it to pack more densely, which along with its larger polarity leads to more effective screening of the electric field from the charged electrode.
- Beyond a critical σ ($\approx$ -12 $\mu C/cm^2$), we find that Li^+ ions tend to accumulate at the graphite edges as the EC/DMC molecules are unable to pack densely enough to shield the charged electrode.
- The predicted potential drop (ϕ) from the graphite electrode to the bulk electrolyte exhibits a nearly linear variation with respect to σ until the onset of Li^+ precipitation at the interface, after which there is no significant variation in ϕ because of the compensation of the additional excess of negative charge on the electrode by the adsorbed Li^+ ions. A brief discussion of how σ is related to the applied voltage is also provided.
- The predicted ΔA gradually increases as Li^+ moves from the bulk-like region to about z = 1 nm from the electrode surface, while its CN changes marginally. This suggests that the Li^+ may remain fully solvated while diffusing through the electrolyte layer. The increasing energy cost results from rearrangements of the Li^+ solvation sheath and its surrounding molecules as the electrolyte becomes more ordered with decreasing z.
- For z < 1 nm, as evidenced by its decreasing CN, the Li^+ may travel as a partially-solvated ion through the densely packed solid-like layer (where solvent molecules are unable to

View Article Online
DOI: 10.1039/C6CP05140E

rearrange to fully solvate it). Therefore, the ΔA sharply increases as the CN of Li^+ continues to decrease unless the electrode charges are sufficient enough to stabilize the partially-desolvated Li^+ ion through favorable electrostatic interactions. Beyond the critical σ ($\approx$ -12 $\mu C/cm^2$), ΔA is predicted to be substantially reduced due to the electrostatic interaction with the negatively charged electrode; in turn this allows the Li^+ to diffuse through the densely packed electrolyte layer followed by its accumulation on the electrode.

- Our analysis shows that the spatial distributions of ions and solvent molecules in the interfacial layer can be substantially perturbed by irregular electrode surfaces with rough edges, Li^+ ions accumulated at the graphite edges, and/or various functional groups. Such perturbation tends to favorably influence Li^+ ion transport through the electrolyte-electrode interface.

In this work, we only focused on the reorganization of solvent molecules (EC and DMC), without considering their decomposition, in the vicinity of the negative electrode at varying applied voltages, including where they may begin to decompose via reduction. Quantitative analysis of the molecular arrangements at the electrolyte-electrode interface helps to better describe electrolyte decomposition/diffusion processes, especially in the initial stages of SEI formation. A better description of the onset of SEI formation is particularly important as it may signficantly influence the growth and structure of SEI layers which are known to be kinetically governed to a large extent.

This study suggests that the interfacial structure can be significantly altered by not only electrolyte composition but also electrode surface modification and operating conditions, warranting further investigations. Such improved mechanistic understanding of the effects of solvent mixture, electrode surface, and operating temperature on the interfacial properties will further assist in efforts to engineer the electrolyte-electrode interface leading to an SEI which

View Article Online
DOI: 10.1039/C6CP05140E

optimizes LIB performance. This work also shows the value of metadynamics as an effective means for evaluating Li^+ ion transport near electrolyte-electrode interfaces. The computational framework presented herein offers a means to explore the interfacial structure and properties for various electrode/electrolyte and operating conditions.

Supporting Information

Electronic supplementary information (ESI) available: Additional available information includes the predicted structural and transport properties of the electrolyte considered (1M $LiPF_6$ in EC:DMC) for validation of the classical force fields employed in this work, in addition to one-dimensional charge density profiles used to estimate the potential difference across the electrolyte-electrode interface as well as the number density profiles for EC, DMC, Li^+ and PF_6^- along the perpendicular direction of the electrode surface at electrode surface charge densities of σ = -4.1 $\mu C/cm^2$ and -8.2 $\mu C/cm^2$.

Acknowledgements

This work was supported by the R.A. Welch Foundation (No. F-1535), Samsung SDI Co., Ltd., and the Korea CCS R&D Center (KCRC) grant (No. 2015053544) funded by the Korea government (Ministry of Science, ICT & Future Planning). We would like to thank the Texas Advanced Computing Center for use of the Stampede supercomputing system (OCI-1134872).

View Article Online
DOI: 10.1039/C6CP05140E

References

1 K. Xu, *Chem. Rev.*, 2004, **104**, 4303–4418.

2 K. Xu, G. V. Zhuang, J. L. Allen, U. Lee, S. S. Zhang, P. N. Ross, and T. R. Jow, *J. Phys. Chem. B*, 2006, **110**, 7708–7719.

3 K. Xu, *Chem. Rev.*, 2014, **114**, 11503–11618.

4 J. B. Goodenough and Y. Kim, *Chem. Mater.*, 2010, **22**, 587–603.

5 M. Armand and J.-M. Tarascon, *Nature*, 2008, **451**, 652–657.

6 B. Scrosati and J. Garche, *J. Power Sources*, 2010, **195**, 2419–2430.

7 E. Peled, *J. Electrochem. Soc.*, 1979, **126**, 2047–2051.

8 E. Peled, *J. Electrochem. Soc.*, 1998, **145**, 3482–3486.

9 D. Aurbach, *Solid State Ionics*, 2002, **148**, 405–416.

10 P. B. Balbuena and Y. Wang, *Lithium-Ion Batteries: Solid-Electrolyte Interphase*, Imperial College Press, 2003.

11 A. Bard and L. Faulkner, *Electrochemical methods: fundamentals and applications*, John Wiley & Sons, 2001.

12 C. Daniel and J. O. Besenhard, *Handbook of Battery Materials*, John Wiley & Sons, 2012.

13 Y. Yamada, Y. Iriyama, T. Abe and Z. Ogumi, *Langmuir*, 2009, **25**, 12766–12770.

14 K. Xu, Y. Lam, S. S. Zhang, T. R. Jow and T. B. Curtis, *J. Phys. Chem. C*, 2007, **111**, 7411–7421.

15 K. Xu, A. von Cresce and U. Lee, *Langmuir*, 2010, **26**, 11538–11543.

16 H. Tavassol, J. W. Buthker, G. A. Ferguson, L. A. Curtiss and A. A. Gewirth, *J. Electrochem. Soc.*, 2012, **159**, A730–A738.

17 I. A. Shkrob, Y. Zhu, T. W. Marin and D. Abraham, *J. Phys. Chem. C*, 2013, **117**, 19255–19269.

18 P. Porion, Y. R. Dougassa, C. Tessier, L. El Ouatani, J. Jacquemin and M. Anouti, *Electrochim. Acta*, 2013, **114**, 95–104.

View Article Online
DOI: 10.1039/C6CP05140E

19 Y. Park, S. H. Shin, H. Hwang, S. M. Lee, S. P. Kim, H. C. Choi and Y. M. Jung, *J. Mol. Struct.*, 2014, **1069**, 157–163.

20 K.-C. Möller, H. J. Santner, W. Kern, S. Yamaguchi, J. O. Besenhard and M. Winter, *J. Power Sources*, 2003, **119-121**, 561–566.

21 N. Leifer, M. C. Smart, G. K. S. Prakash, L. Gonzalez, L. Sanchez, K. A. Smith, P. Bhalla, C. P. Grey and S. G. Greenbaum, *J. Electrochem. Soc.*, 2011, **158**, A471–A480.

22 Y. Kameda, Y. Umebayashi, M. Takeuchi, M. A. Wahab, S. Fukuda, S. Ishiguro, M. Sasaki, Y. Amo and T. Usuki, *J. Phys. Chem. B*, 2007, **111**, 6104–6109.

23 Y.-K. Han, Y. Moon, K. Lee and Y. S. Huh, *Curr. Appl. Phys.*, 2014, **14**, 897–900.

24 G. Gourdin, J. Collins, D. Zheng, M. Foster and D. Qu, *J. Phys. Chem. C*, 2014, **118**, 17383–17394.

25 F. German, A. Hintennach, A. LaCroix, D. Thiemig, S. Oswald, F. Scheiba, M. J. Hoffmann and H. Ehrenberg, *J. Power Sources*, 2014, **264**, 100–107.

26 S. Chattopadhyay, A. L. Lipson, H. J. Karmel, J. D. Emery, T. T. Fister, P. A. Fenter, M. C. Hersam and M. J. Bedzyk, *Chem. Mater.*, 2012, **24**, 3038–3043.

27 G. Bieker, M. Winter and P. Bieker, *Phys. Chem. Chem. Phys.*, 2015, **17**, 8670–8679.

28 L. O. Valøen and J. N. Reimers, *J. Electrochem. Soc.*, 2005, **152**, A882–A891.

29 R. Bhattacharyya, B. Key, H. Chen, A. S. Best, A. F. Hollenkamp and C. P. Grey, *Nat. Mater.*, 2010, **9**, 504–510.

30 M. K. Petersen, R. Kumar, H. S. White and G. A. Voth, *J. Phys. Chem. C*, 2012, **116**, 4903–4912.

31 J. Yu, P. B. Balbuena, J. Budzien and K. Leung, *J. Electrochem. Soc.*, 2011, **158**, A400–A410.

32 L. Xing and O. Borodin, *Phys. Chem. Chem. Phys.*, 2012, **14**, 12838–12843.

33 J. Cheng and M. Sprik, *Phys. Chem. Chem. Phys.*, 2012, **14**, 11245–11267.

34 K. Leung, *Chem. Phys. Lett.*, 2013, **568-569**, 1–8.

35 K. Leung, *Phys. Chem. Chem. Phys.*, 2015, **17**, 1637–1643.

36 O. Borodin and G. D. Smith, *J. Phys. Chem. B*, 2009, **113**, 1763–1776.

View Article Online
DOI: 10.1039/C6CP05140E

37 J. Vatamanu, O. Borodin and G. D. Smith, *J. Phys. Chem. C*, 2012, **116**, 1114–1121.

38 R. Jorn, R. Kumar, D. P. Abraham and G. A. Voth, *J. Phys. Chem. C*, 2013, **117**, 3747–3761.

39 C. E. Banks, T. J. Davies, G. G. Wildgoose and R. G. Compton, *Chem. Commun. (Camb).*, 2005, 829–841.

40 T. R. Jow, K. Xu, O. Borodin and M. Ue, *Electrolytes for Lithium and Lithium-Ion Batteries*, Springer New York, New York, NY, 2014, vol. 58.

41 N. A. McDonald and W. L. Jorgensen, *J. Phys. Chem. B*, 1998, **102**, 8049–8059.

42 R. C. Rizzo and W. L. Jorgensen, *J. Am. Chem. Soc.*, 1999, **121**, 4827–4836.

43 M. L. P. Price, D. Ostrovsky and W. L. Jorgensen, *J. Comput. Chem.*, 2001, **22**, 1340–1352.

44 B. Hess, C. Kutzner, D. van der Spoel and E. Lindahl, *J. Chem. Theory Comput.*, 2008, **4**, 435–447.

45 G. J. Martyna, D. J. Tobias and M. L. Klein, *J. Chem. Phys.*, 1994, **101**, 4177–4189.

46 G. J. Martyna, M. E. Tuckerman, D. J. Tobias and M. L. Klein, *Mol. Phys.*, 1996, **87**, 1117–1157.

47 G. J. Martyna, M. L. Klein and M. Tuckerman, *J. Chem. Phys.*, 1992, **97**, 2635–2643.

48 A. Laio and M. Parrinello, *Proc. Nat. Acad. Sci. USA*, 2002, **99**, 12562–12566.

49 A. Barducci, G. Bussi and M. Parrinello, *Phys. Rev. Lett.*, 2008, **100**, 020603.

50 G. A. Tribello, M. Bonomi, D. Branduardi, C. Camilloni and G. Bussi, *Comput. Phys. Commun.*, 2014, **185**, 604–613.

51 E. Paek, A. J. Pak and G. S. Hwang, *J. Electrochem. Soc.*, 2012, **160**, A1–A10.

52 A. J. Pak, E. Paek and G. S. Hwang, *J. Phys. Chem. C*, 2014, **118**, 21770–21777.

53 K. Leung and J. L. Budzien, *Phys. Chem. Chem. Phys.*, 2010, **12**, 6583.

54 J. M. Rosolen, *J. Electrochem. Soc.*, 1996, **143**, 2417.

55 M. S. Hossain, D. Tryk and E. Yeager, *Electrochim. Acta*, 1989, **34**, 1733–1737.

56 S. Megahed and B. Scrosati, *J. Power Sources*, 1994, **51**, 79–104.

View Article Online
DOI: 10.1039/C6CP05140E

57 S. A. Delp, O. Borodin, M. Olguin, C. G. Eisner, J. L. Allen and T. R. Jow, *Electrochim. Acta*, 2016, **209**, 498–510.

58 E. Paek, A. J. Pak, K. E. Kweon and G. S. Hwang, *J. Phys. Chem. C*, 2013, **117**, 5610–5616.

59 E. Paek, A. J. Pak and G. S. Hwang, *J. Chem. Phys.*, 2015, **142**, 024701.

View Article Online
DOI: 10.1039/C6CP05140E

Table of Contents